



HAL
open science

Multiple-Photon Resonance Enabled Quantum Interference in Emission Spectroscopy of N₂⁺

Xiang Zhang, Qi Lu, Yalei Zhu, Jing Zhao, Rostyslav Danylo, Liang Xu, Mingwei Lei, Hongbing Jiang, Chengyin Wu, Zhedong Zhang, et al.

► **To cite this version:**

Xiang Zhang, Qi Lu, Yalei Zhu, Jing Zhao, Rostyslav Danylo, et al.. Multiple-Photon Resonance Enabled Quantum Interference in Emission Spectroscopy of N₂⁺. *Ultrafast Science*, 2024, 4, pp.0051. 10.34133/ultrafastscience.0051 . hal-04376919

HAL Id: hal-04376919

<https://ensta-paris.hal.science/hal-04376919>

Submitted on 7 Jan 2024

HAL is a multi-disciplinary open access archive for the deposit and dissemination of scientific research documents, whether they are published or not. The documents may come from teaching and research institutions in France or abroad, or from public or private research centers.

L'archive ouverte pluridisciplinaire **HAL**, est destinée au dépôt et à la diffusion de documents scientifiques de niveau recherche, publiés ou non, émanant des établissements d'enseignement et de recherche français ou étrangers, des laboratoires publics ou privés.



Distributed under a Creative Commons Attribution 4.0 International License

RESEARCH ARTICLE

Multiple-Photon Resonance Enabled Quantum Interference in Emission Spectroscopy of N_2^+

Xiang Zhang^{1†}, Qi Lu^{1†}, YaLei Zhu², Jing Zhao^{2*}, Rostyslav Danylo^{1,3}, Liang Xu¹, Mingwei Lei⁴, Hongbing Jiang⁴, Chengyin Wu⁴, Zhedong Zhang⁵, Aurélien Houard³, Vladimir Tikhonchuk^{6,7}, André Mysyrowicz³, Qihuang Gong⁴, Songlin Zhuang¹, Zengxiu Zhao², and Yi Liu^{1,8*}

¹Shanghai Key Lab of Modern Optical System, University of Shanghai for Science and Technology, 516, Jungong Road, 200093 Shanghai, China. ²Department of Physics, National University of Defense Technology, Changsha 410073, China. ³Laboratoire d'Optique Appliquée, ENSTA Paris, Ecole Polytechnique, CNRS, Institut Polytechnique de Paris, 828 Boulevard des Maréchaux, 91762 Palaiseau Cedex, France. ⁴State Key Laboratory for Mesoscopic Physics, School of Physics, Peking University, Beijing 100871, China. ⁵Department of Physics, City University of Hong Kong, Kowloon, Hong Kong SAR. ⁶Centre Lasers Intenses et Applications, University of Bordeaux-CNRS-CEA, 351 Cours de la Liberation, 33405 Talence Cedex, France. ⁷Extreme Light Infrastructure ERIC, ELI Beamlines Facility, 25241 Dolní Břežany, Czech Republic. ⁸CAS Center for Excellence in Ultra-intense Laser Science, Shanghai 201800, China.

*Address correspondence to: jzhao@nudt.edu.cn (J.Z.); yi.liu@usst.edu.cn (Y.L.)

†These authors contributed equally to this work.

Quantum interference occurs frequently in the interaction of laser radiation with materials, leading to a series of fascinating effects such as lasing without inversion, electromagnetically induced transparency, Fano resonance, etc. Such quantum interference effects are mostly enabled by single-photon resonance with transitions in the matter, regardless of how many optical frequencies are involved. Here, we report on quantum interference driven by multiple photons in the emission spectroscopy of nitrogen ions that are resonantly pumped by ultrafast infrared laser pulses. In the spectral domain, Fano resonance is observed in the emission spectrum, where a laser-assisted dynamic Stark effect creates the continuum. In the time domain, the fast-evolving emission is measured, revealing the nature of free-induction decay arising from quantum radiation and molecular cooperativity. These findings clarify the mechanism of coherent emission of nitrogen ions pumped with mid-infrared pump laser and are found to be universal. The present work opens a route to explore the important role of quantum interference during the interaction of intense laser pulses with materials near multiple photon resonance.

Introduction

Quantum interference is traditionally observed with weak laser field (below threshold field for ionization) resonantly interacting with materials. With laser field close to or more intense than the threshold field for ionization of atoms or molecules, $\sim 10^{13}$ W/cm², it was believed that the ionization and plasma formation would destroy the coherence of the system [1–3]. However, this turns out to be not true. In recent studies of strong-field interaction with molecules, dielectric materials and 2-dimensional semiconductors, it has been shown that quantum interference and coherence may contribute importantly [4–6]. Quantum coherence is evidenced in the cavity-free lasing of air molecules pumped with intense femtosecond pulses, where the crucial role of the electronic, vibrational, and rotational motions of molecules, and their couplings is highlighted [7–10]. Cavityless lasing of nitrogen molecules in ambient air holds unique potential to generate a virtual lasing source in the sky,

where a coherent optical beam is emitted by the air plasma from the sky toward the ground observer [7]. In spite of many efforts [3,7–20], the physical mechanism of cavityless lasing of N_2^+ is still controversial. In particular, there is still a debate on the nature of the radiation obtained with different pump laser frequencies, ranging from mid-infrared regime (3.9 μm , 2.6 to 1.1 μm) to near-infrared at 800 nm, and even ultraviolet light at 400 nm.

In this work, we examine the forward 391.4-nm coherent emission corresponding to the transition of N_2^+ pumped by a mid-infrared wavelength tunable femtosecond pulses in the spectral and temporal domain. In the emission spectrum, a Fano line shape and a broadband continuum are observed under proper conditions. To obtain the temporal profile of the emission, we used a cross-correlation method based on sum-frequency generation (SFG) of the emission signal with a weak probe pulse. It was found that the 391.4-nm emission presents a pressure-independent monotonous decaying waveform of

Citation: Zhang X, Lu Q, Zhu Y, Zhao J, Danylo R, Xu L, Lei M, Jiang H, Wu C, Zhang Z, et al. Multiple-Photon Resonance Enabled Quantum Interference in Emission Spectroscopy of N_2^+ . *Ultrafast Sci.* 2024;4:Article 0051. <https://doi.org/10.34133/ultrafastscience.0051>

Submitted 31 August 2023
Accepted 7 November 2023
Published 5 January 2024

Copyright © 2024 Xiang Zhang et al. Exclusive licensee Xi'an Institute of Optics and Precision Mechanics. No claim to original U.S. Government Works. Distributed under a Creative Commons Attribution License 4.0 (CC BY 4.0).

several-picoseconds duration, following fifth/third harmonics generation of a few-hundred-femtoseconds duration. Our measurements of the emission spectrum reveal the important role of quantum interference between a direct transition channel and a continuum induced by the dynamic Stark effect. We attribute the nature of the direct coherent forward emission to free-induction decay (FID), enabled by 3- or 5-photon resonant excitation. An intense narrowband emission is observed in CO₂ gas as well, suggesting the universality of quantum interference and FID driven by multiple-photon resonance.

Methods

The experimental setup is presented in Fig. 1. In our experiments, femtosecond laser pulses (12 mJ, 800 nm, 40 fs, 1 kHz, Legend DUO, Coherent Ltd) from a commercial laser system were first split into an intense and a weaker pulse, with a dielectric beam splitter. The pulse of 5-mJ energy was used to pump a commercial optical parametric amplifier (OPA, TOPAS, Coherent Ltd) which produced MIR femtosecond pulses tunable from 1.1 to 2.6 μm, with a pulse energy ranging from 30 to 650 μJ. The pulse duration of these MIR pulses was 1.5 times of the incident 800-nm pump pulses. They were focused by a convex lens of $f = 35$ or 50 mm into ambient air or a gas chamber filled with nitrogen gas at different pressures. A gas plasma of ~2- to 5-mm length was formed, which gave rise to intense forward 391.4- and/or 427.8-nm emissions. The emissions after the strong nonlinear interaction with the plasma were collimated by another lens of $f = 10$ mm. To filter out the strong fundamental MIR pulse and the accompanying white-light emission, the pulse was reflected successively on 2 dichromatic mirrors, which transmit only spectral components below 550 nm. In a first experiment, the radiation below 550 nm was collected into a fiber tip connected to a spectrometer for spectral measurements. In a second experiment, the 391.4-nm radiation was focused onto a SFG BBO crystal (cut angle = 44.3°) together with the second weaker pulse at 800 nm with an energy of ~50 μJ. The SFG signal at 263 nm was recorded as a function of the

relative delay between the 391.4-nm radiation and the probe pulse, to resolve the 391.4-nm radiation in the temporal domain.

Results and Discussion

We present the spectrum of the forward emission for different pump laser wavelengths λ_0 in Fig. 2. The broadband emission around 370 to 450 nm in Fig. 2A, showing a red shift with increasing pump laser wavelength, corresponds to the third harmonic of the MIR pump laser. More importantly, intense narrow lines around 391.4 and 427.8 nm, corresponding to the transition of $B^2\Sigma_u^+$ ($\nu' = 0$) to the $X^2\Sigma_g^+$ ($\nu = 0, 1$) states of nitrogen ions, appear for a pump laser wavelength between 1,150 and 1,320 nm. This agrees with previously reported observations [14]. The relevant energy levels of the nitrogen ions are depicted in Fig. 1B. For a pump laser wavelength tuned between 1,530 and 1,890 nm, a strong emission around 391.4 nm and a relatively weaker one around 358.2 nm (corresponding to transition between $B^2\Sigma_u^+$ ($\nu' = 1$) to the $X^2\Sigma_g^+$ ($\nu = 0$)) can be observed, as presented in Fig. 2B and C. The broadband emission situated around 480 to 550 nm and 360 to 380 nm in Fig. 2B and C corresponds to the third and the fifth harmonics of the MIR pump laser, respectively. It should be noted that the focusing conditions and the gas pressures in Fig. 2A to C are not identical due to that we have systematically optimized the emission signal for the 3 ranges of pump laser wavelength, especially in view that the available pump pulses energy varies significantly for such a broad tuning range of pump pulse wavelength. These results are summarized in Fig. 3A and compared with simulations, which will be detailed later on.

We notice that the intensity of the narrow-line 391.4-nm radiation relative to the intensity of the third/fifth harmonics depends on the pump pulse energy, focusing geometry, and gas pressure. By optimizing the pump laser energy and gas pressure, we observed 2 key features in the spectral domain. For a pump laser wavelength $\lambda_0 = 1,170$ nm with a moderate incident energy of 32 μJ, a Fano line shape can be observed clearly in ambient air, as presented in Fig. 4A, while for $\lambda_0 = 1,800$ nm,

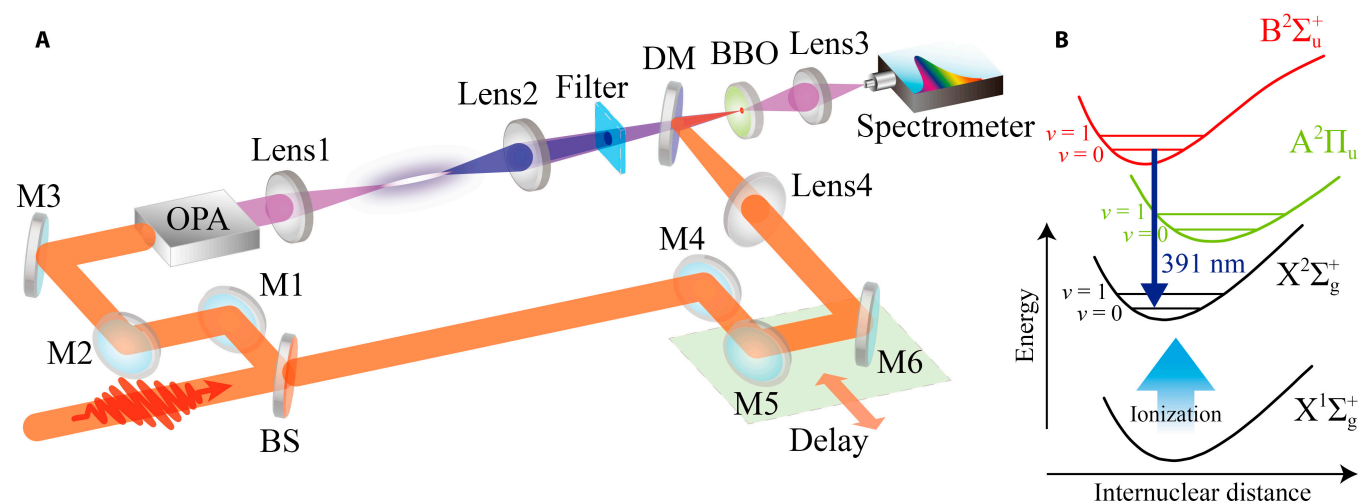


Fig. 1. (A) The femtosecond laser pulses pump the OPA, which provides tunable femtosecond pulses ranging from 1,100 nm to 2,600 nm. The OPA output pulses pump nitrogen gas and create the plasma. The forward coherent emission from the plasma was filtered and mixed with a weak probe pulse into a BBO crystal for its characterization. (B) The schematic energy levels of the nitrogen ion.

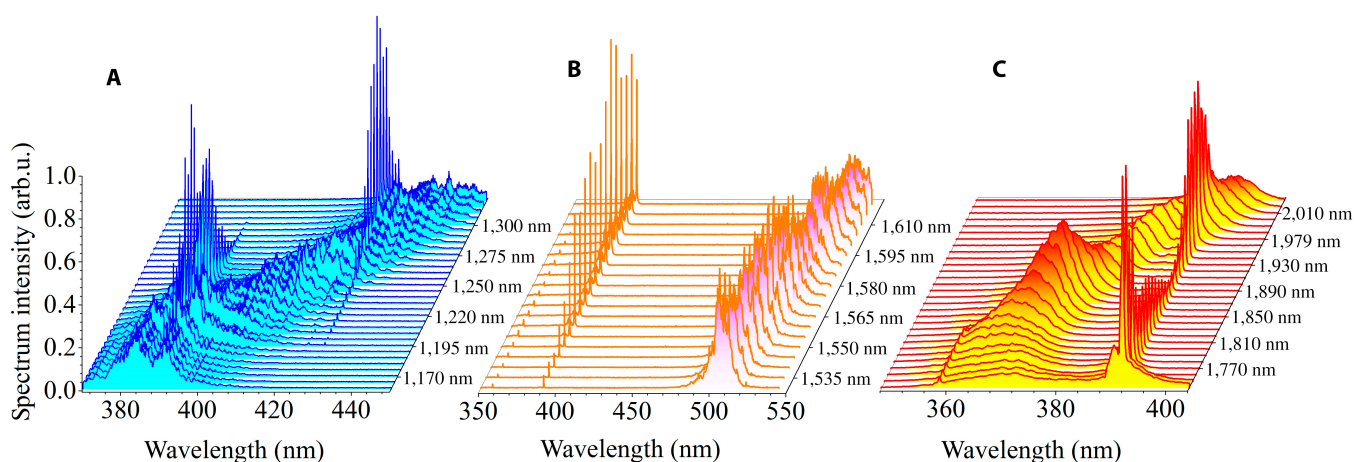


Fig. 2. Spectrum of the forward emission obtained by different pump laser wavelengths. The wavelength of the pump laser is indicated on the right side of each panel. In (A) and (B), the nitrogen gas pressure was 30 mbar, while in (C), ambient air at 1 bar was used. The pump pulse energy was respectively 70, 90, and 300 μJ for (A) to (C). In (A) and (B), focal lens of $f = 30$ mm was used while in (C) $f = 50$ mm.

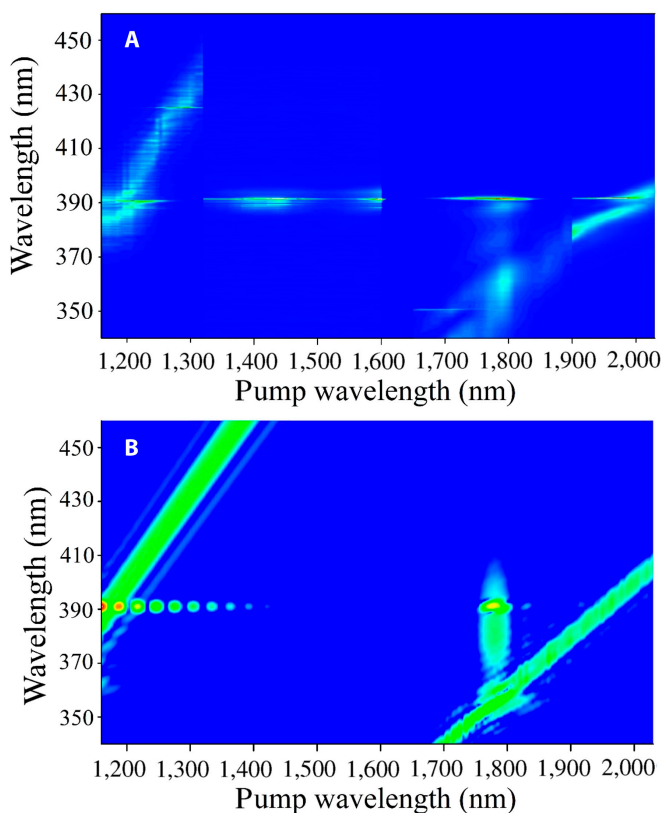


Fig. 3. Spectrum intensity for different pump laser wavelengths. (A) Experimental results and (B) calculated results. The experimental parameters are the same as in Fig. 2. For the simulation, the laser intensity was $1.3 \times 10^{14} \text{ W/cm}^2$, which corresponds to the enhancement at 1,800 nm.

we found a continuum between the fifth harmonic and the 391.4-nm radiation, as depicted in Figs. 3A and 4B.

To gain deeper understanding on the nature of the intense 391.4-nm emission, we performed time-resolved measurements using the cross-correlation technique [16]. Figure 5 presents the experimental measurements of the 391.4-nm signal for the pump laser wavelength of 1,950 and 1,550 nm. The time-resolved

sum frequency signal of the 391.4-nm signal and the weak 800-nm probe pulse are presented in Fig. 5A and D. At 1,950 nm with a pump pulse energy of $E_{\text{in}} = 200 \mu\text{J}$, the 391.4-nm emission is not visible so that the fifth harmonic dominates, as shown in Fig. 5C. In the temporal domain, the fifth harmonic emission shows a short duration of 250 fs (Fig. 5B), as expected from the harmonic generation process. By further increasing the pulse energy, the 391.4-nm emission becomes prominent and finally dominates in the spectrum (Fig. 5C). Notably, in the temporal domain, following the fifth harmonics, a monotonous decay of emission profile extending to 4 ps is observed. For $\lambda_0 = 1,550$ nm whose third and fifth harmonics are far away from the 391.4-nm spectrum range, the emission shows a clean temporal profile during 2 to 3 ps (10% level), as given in Fig. 5E. Moreover, we examined the influence of nitrogen gas pressure, keeping the pump wavelength fixed at 1,550 nm. The temporal profile of the emission does not show significant changes within the range of gas pressure from 20 to 70 mbar. Therefore, it rules out a super-radiance mechanism that should present an emission built-up time within picoseconds and an emission lifetime scaling with the inverse of gas pressure [16,19,20].

In support of our measurements, we propose a theoretical model based on the quantum theory of harmonic generation [21] describing the emission spectra of nitrogen molecules subject to a MIR laser pulse, without consideration of the propagation effect. Once the nitrogen ions are created by strong-field ionization, the influence of the free electrons on the coherence of the ions can only persist for several femtoseconds as demonstrated in [22]. Thus, we focus on the coherent emission of N_2^+ . By considering the ionic excited state B, the time-dependent wave packet of N_2^+ becomes the coherent superposition of the ionic ground state $|\varphi_X\rangle$, the excited state $|\varphi_B\rangle$ and the continuum state $|k\rangle$, i.e., $|\varphi_X\rangle = a_X(t)|\varphi_X\rangle + a_B(t)|\varphi_B\rangle + \int dk a_k(t)|k\rangle$. We generalize the theory in [21] with 2-state coupled equation [3,23] to describe the coupling between the ionic ground state $X^2\Sigma_g^+$ and the excited state $B^2\Sigma_u^+$,

$$i\frac{\partial}{\partial t} \begin{pmatrix} a_X(t) \\ a_B(t) \end{pmatrix} = \begin{pmatrix} \varepsilon_X & -\mu E(t) \\ -\mu E(t) & \varepsilon_B \end{pmatrix} \begin{pmatrix} a_X(t) \\ a_B(t) \end{pmatrix} \quad (1)$$

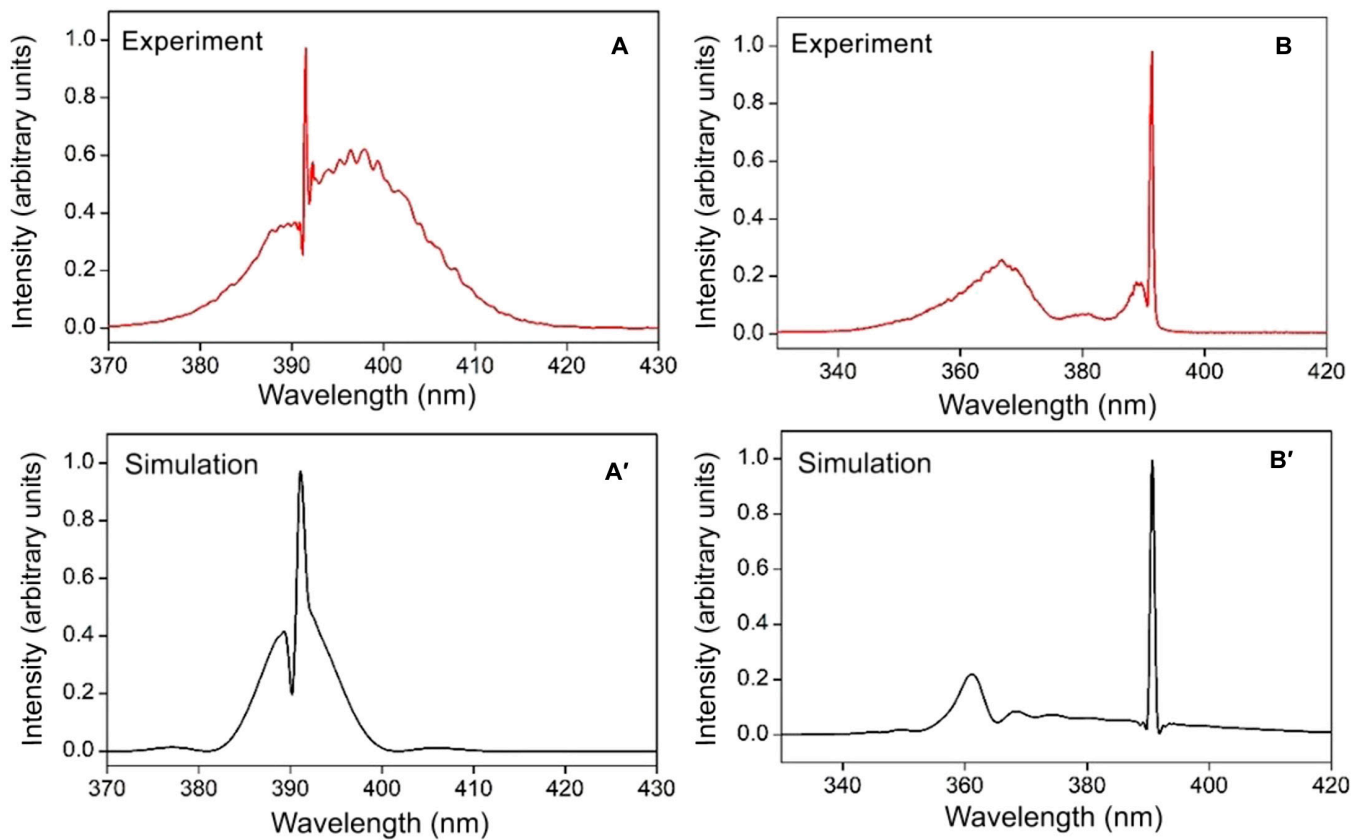


Fig. 4. (A) Spectrum of the forward emission with $\lambda_0 = 1,170$ nm, with pulse energy of $32 \mu\text{J}$ and 1 bar air used. (B) Spectrum in case of $\lambda_0 = 1,800$ nm. The pump pulse energy was $40 \mu\text{J}$ and air is used. (A') and (B') corresponding simulation results. The simulation parameters are the same as in Fig. 2.

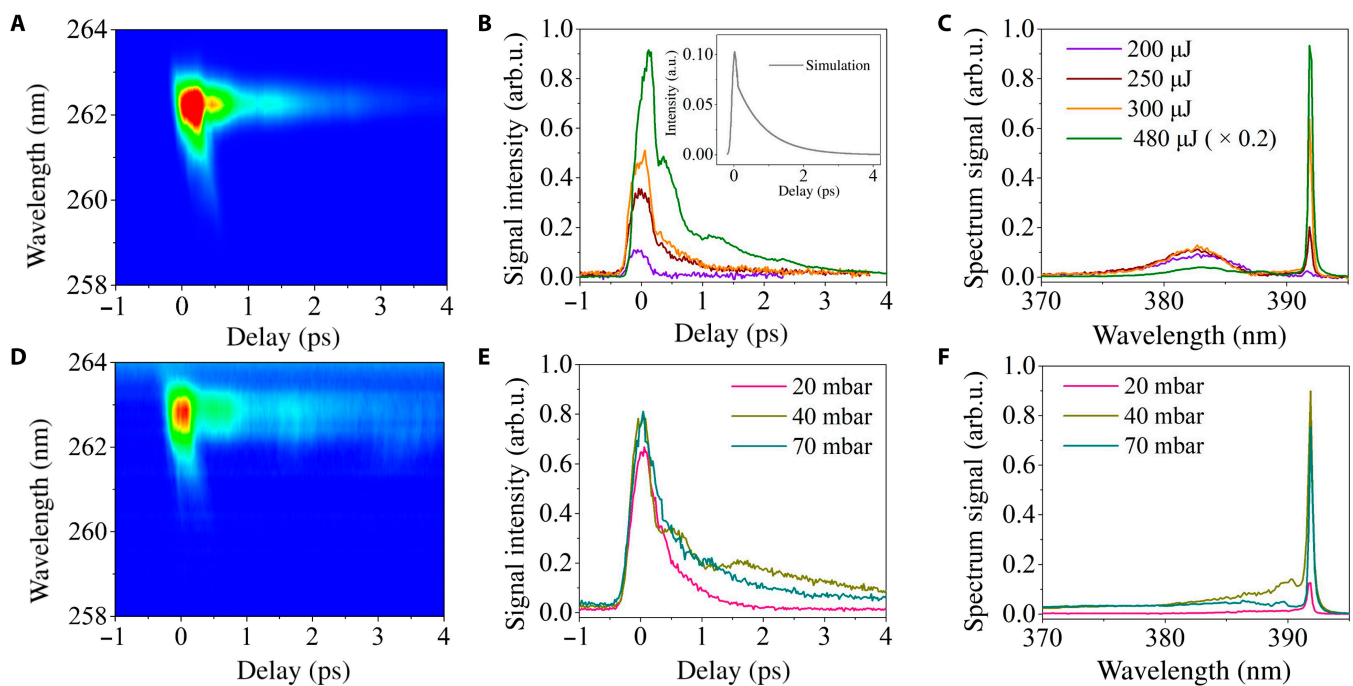


Fig. 5. (A) Time resolved measurement of the sum-frequency signal between the 391.4-nm emission and the weak 800-nm probe pulse. (B) Temporal profile of the 391.4-nm emission. (C) Spectrum of the forward emission corresponding to (B). In (B) and (C), the temporal profile measurement and spectrum intensity in case of $E_{in} = 480 \mu\text{J}$ are multiplied by some factors for easier comparison with other energies. The pump laser wavelength for (A) to (C) is 1,950 nm. For (D) to (F), the pump laser wavelength is 1,550 nm.

where $\varepsilon_{X,B}$ and $a_{X,B}(t)$ denote the energies and the amplitudes of the ionic states $X^2 \Sigma_g^+$ and $B^2 \Sigma_u^+$ with the vibrational quantum number $v' = v = 0$. The energy of the excited state B is a complex value with its imaginary part describing the dephasing time of the FID emission, which can be estimated from the time-resolved measurements in Fig. 4. The nondiagonal terms describe the coupling between the 2 ionic states with the transition matrix element of $\mu = |\langle \varphi_B | r | \varphi_X \rangle| \approx 1.5D$ [24]. For simplicity, we assume that the ions are prepared in the ground state $X^2 \Sigma_g^+$, and the electric field $E(t)$ felt by the ions is ramped-up smoothly over 1.5 cycles from zero to the peak of the field strength. The pulse duration used in the simulation is twenty optical cycles with Gaussian envelope. The free electrons are assumed to be ionized from the ionic ground state and the direct ionization from the excited state is neglected due to its relatively low population. The interaction between the continuum electrons and the bound electrons is neglected because their coherence can persist only for several femtoseconds, which plays important role in recollision-induced dynamics [16]. The amplitude of the continuum state $a_k(t)$ is derived by following Eq. 5 in [21] with the inclusion of $a_X(t)$,

$$a_k(t) = -i \int_0^t dt' e^{-iS(k,t,t')} a_X(t') E(t') d_X(k+A(t')) \quad (2)$$

with the classical action acquired by the electron during excursion in the continuum state $S(k,t,t') = \int_{t'}^t d\tau \left[\frac{(k+A(\tau))^2}{2} + I_p \right]$ and $A(t)$ is the vector potential of the laser field. $d_X(k+A(t')) = \langle k+A(t') | r | \varphi_X \rangle$ describes the transition amplitude from the ionic ground state X to the continuum state at ionization time t' . By solving Eq. (1) and Eq. (2) numerically, we obtain the time-dependent dipole moment,

$$d(t) \approx \int dka_X^*(t) a_k(t) d_X(k+A(t)) + a_X^*(t) a_B(t) \mu \quad (3)$$

The first term describes the transition between the state X and the continuum, and the second term represents the transition between the 2 bound states. As a result, the full emission of N_2^+ involves harmonic generation from the ions and coherent emission from the laser-coupled 2-level states. The emission spectrum can be obtained from the Fourier transform of the time-dependent dipole moment.

The calculated emission spectrum is plotted in Fig. 3B. The broadband harmonics and the narrowband 391.4-nm emission show a strong dependence on the pump laser wavelength, in good agreement with experiments. When the third or fifth harmonic spectrum approaches the wavelength of 391.4 nm, the interference between the 2 transition pathways results in the asymmetric Fano line shape in the spectra [25,26]. In the time domain, the dipole moment of N_2^+ is the sum of the harmonic emission described by a function of $H(t)$ and the FID emission with an exponentially decaying dipole moment oscillating with frequency ω_{XB} and decay width Γ ,

$$d(t) \propto a_h H(t) + \exp\left(-i\omega_{XB}t - \frac{\Gamma}{2}t + i\phi\right) \quad (4)$$

The scaling factor a_h represents the intensity ratio of the harmonic and the narrowband emission, and they have a phase delay of ϕ . For harmonics, the radiation process occurs within attoseconds and repeats every half-cycle of the laser pulse. For

the narrowband emission, it lasts for several picoseconds. Thus, the harmonic dipole function $H(t)$ can be considered as a Dirac delta function $\delta(t)$. In the spectral domain, the interference between the harmonic and the narrowband emissions could yield the Fano line shape, and the Fano asymmetry parameter is determined by the phase delay by $q = -\cot(\phi/2)$ [25]. The harmonics originate from the transition between field-dressed bound states during the laser pulse. Their frequencies are determined by the instantaneous Stark-shifted transition energies between X and B states induced by the laser coupling, thus providing a broadband background. The spectral profile is determined by the relative intensity and phase between the 2 transitions, which are sensitive to the laser intensity. Taking an appropriate ratio of amplitude and phase difference between the 391.4-nm emission and the broadband fifth harmonic, the Fano feature can be reproduced in Fig. 4A'. In Fig. 3B, a periodic oscillation of the 391.4-nm emission can be noticed. The origin of this behavior is due to the Rabi oscillation of the population in the B state driven by the laser pulse, which is sensitive to the wavelength and intensity of the pump laser used in the simulation. However, in the experiments this oscillatory behavior can be somehow washed out due to the averaging of lasing intensity in the focal zone of the pump laser.

The simulation reproduces the observation that the fifth harmonic and the 391.4-nm signal are enhanced at the wavelength around 1,800 nm, which deviates from the field-free 5-photon resonant wavelength of 1,957 nm. This difference can be attributed to the dynamic Stark shift induced by the laser-coupling of the X and B states. When the MIR pulse interacts with the nitrogen ions, the energy levels follow the field adiabatically and return to their proper values after the pulse. The energy shift between these 2 levels depends on the laser intensity as $\Delta\varepsilon_{XB}(t) \approx \frac{2\mu^2}{\hbar\omega} E^2(t)$. Here, ω is the frequency of the laser field. The population at the B state is efficiently enhanced when the driving field couples the X and B states, that is, when the third or fifth harmonic approaches the energy difference between the levels, $\varepsilon_B - \varepsilon_X + \Delta\varepsilon_{XB}$. For example, the laser intensity of 1.3×10^{14} W/cm² corresponds to an optical period averaged energy shift of $\Delta\varepsilon_{XB} \approx 0.265$ eV. This value matches well 5 times of the energy difference of 0.055 eV between the 1,957 and 1,800 nm, which corresponds to the resonant coupling to the fifth harmonic at the wavelength of 1,800 nm, instead of 1,957 nm in the absence of the Stark effect.

The role of the dynamic Stark shift in the excitation of B level is confirmed by a comparison of the emission spectra around 391.4 nm for 2 values of laser energy of 70 and 140 μ J in Fig. 6. For lower incident energy of 70 μ J the optimum pump wavelength was observed to be 1,830 nm, while it shifts to 1,800 nm for $E_{in} = 140$ μ J. The shift of the optimum wavelength for increasing pump laser intensity is in good agreement with the theoretical predictions, confirming the role of dynamic Stark effect. Since the dynamic Stark effect depends on time, the energy difference between B and X states spans a range between the field-free value $\varepsilon_B - \varepsilon_X$ and the maximum shift $\varepsilon_B - \varepsilon_X + \Delta\varepsilon_{XB}$. As shown in Fig. 3, around $\lambda_0 = 1,800$ nm the Stark shift spans the wavelength range from 391.4 to 358.2 nm, which explains the excitation of the emission at 358.2 nm observed in the experiment and in the theory.

The intense narrowband emission, the asymmetrical Fano line shape and the picosecond duration of the emission are the signatures of FID, as reported in the visible and extreme

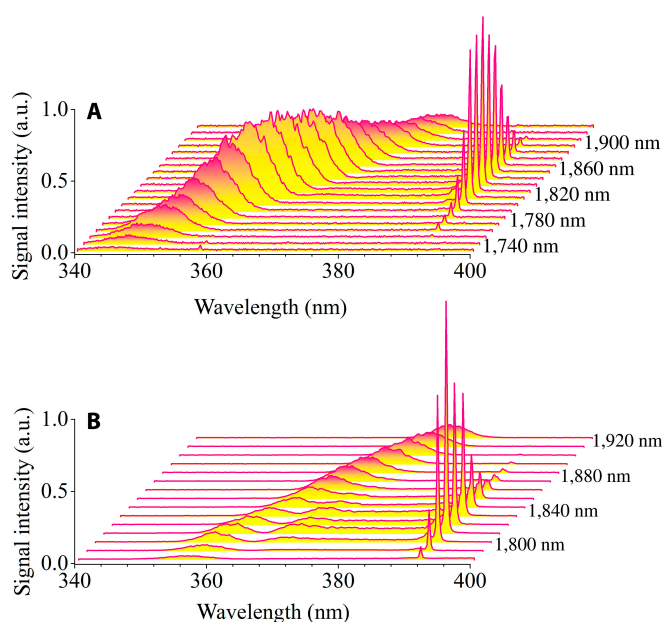


Fig. 6. Stark effect in the lasing emission. The pump laser energies were 70 and 140 μJ for (A) and (B). The gas is pure nitrogen of 1 bar. The optimal wavelength for 391.4-nm signal was 1,830 nm in (A) and 1,810 nm in (B).

ultraviolet regimes [27–30]. FID is the emission following the coherent excitation of a resonant level that was earlier observed in nuclear magnetic resonance and later in optical domain [27,30]. We support our hypothesis of FID with additional evidences in 2 aspects. In FID process, there exists no population inversion of the corresponding excited and ground states and no optical gain is expected for an externally injected seeding pulse. We confirmed this fact by injecting a seed pulse into the air plasma pumped by a 1,900-nm femtosecond pulse: no amplification of the seed pulse was observed, in agreement with the previous reports [13]. Secondly, the FID effect is expected to be universal for atoms or molecules when an intrinsic optical transition between 2 electronic levels is resonantly driven by MIR pump laser. Inspired by the observation of Chu et al. [31], we pumped CO_2 gas with femtosecond laser at 1,600 nm. The experimental results are presented in Fig. 7. The narrow emission peak located around 337 nm can be attributed to the FID transition of $A^2\Pi_u$ ($\nu = 1$) to $X^2\Pi_g$ ($\nu' = 0$) of CO_2^+ , while the broad band emission around 325 nm is the fifth harmonic of the pump laser. It will be interesting to look for other gas species in which such FID effect can be observed.

Conclusion

In summary, we have performed measurements of the intense coherent forward emission at 391.4 nm of nitrogen ions pumped by mid-infrared femtosecond pulses in the spectral and temporal domain. An asymmetric Fano line shape and a broad continuum bridging the intense 391.4-nm radiation with the fifth harmonic are observed. Time-resolved measurements revealed that the 391.4-nm pulses show a pressure-independent pulse duration of a few picoseconds, which is intrinsically different from the superradiant 391.4-nm emission in case of pumping with 800-nm laser. We attribute this forward 391.4-nm emission to a FID of nitrogen ions, where the B-X transition was resonantly driven by a 3- or 5-photon process. Our theoretical

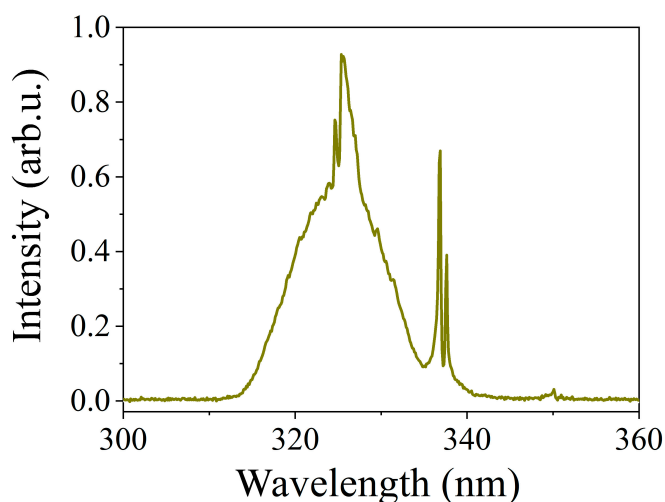


Fig. 7. FID signal in CO_2 . Forward emission spectrum obtained in CO_2 gas pumped by MIR pulse at 1,600 nm. The pulse energy was 85 μJ , and the gas pressure was 100 mbar.

model based on the strong field approximation reproduces well the intense emission at 391.4 nm, the Fano line shape, as well as the spectral continuum with pump laser at wavelength of 1,800 nm. We believe that FID effect should universally exist in atoms or molecules when their intrinsic transitions are resonantly excited by intense femtosecond laser pulse, which is confirmed by observations in CO_2 .

Acknowledgments

Funding: The work is supported in part by the National Natural Science Foundation of China (Grant Nos. 12034013, 12234020, 12204308, 12174011, and 12104380), the Shanghai Science and Technology Commission (Grant No. 22ZR1444100), and the Early Career Scheme (No. 9048216) and NSFC/RGC Collaborative Research Scheme (No. 9054901) from the Research Grants Council of Hong Kong.

Author contributions: Y.L., Z. Zhang, S.Z., Q.G., and A.M. conceived the idea and designed the experiments. X.Z., Q.L., R.D., and M.L. conducted the experiments. Y.Z., J.Z., and Z. Zhao performed the numerical simulations. Y.L., H.J., C.W., Z. Zhang, A.H., V.T., A.M., and Z. Zhao analyzed the data. Y.L., X.Z., J.Z., Z. Zhang, A.M., and Z. Zhao wrote the paper, and it was discussed among all authors.

Competing interests: The authors declare that they have no competing interests.

Data Availability

The data that support the plots within this paper will be available from the corresponding authors upon reasonable request.

References

1. Vacher M, Bearpark MJ, Robb MA, Malhado JP. Electron dynamics upon ionization of polyatomic molecules: Coupling to quantum nuclear motion and decoherence. *Phys Rev Lett.* 2017;118(8):Article 083001.
2. Pabst S, Greenman L, Ho PJ, Mazziotti DA, Santra R. Decoherence in attosecond photoionization. *Phys Rev Lett.* 2011;106(5):Article 053003.

3. Zhang Q, Xie H, Li G, Wang X, Lei H, Zhao J, Chen Z, Yao J, Chen Y, Zhao Z. Sub-cycle coherent control of ionic dynamics via transient ionization injection. *Commun Phy.* 2020;3:50.
4. Gorlach A, Neufeld O, Rivera N, Cohen O, Kammer I. The quantum-optical nature of high harmonic generation. *Nat Commun.* 2020;11:4598.
5. Gombkőto Á, Varró S, Mati P, Földi P. High-order harmonic generation as induced by a quantized field: Phase-space picture. *Phys Rev A.* 2020;101(1):Article 013418.
6. Lewenstein M, Ciappina MF, Pisanty E, Rivera-Dean J, Stammer P, Lamprou T, Tzallas P. Generation of optical Schrödinger cat states in intense laser-matter interactions. *Nat Photon.* 2021;17:1104–1108.
7. Yuan L, Liu Y, Yao J, Cheng Y, Cheng Y. Recent advances in air lasing: A perspective from quantum coherence. *Adv Quantum Technol.* 2019;2:1900080.
8. Ando T, Lötstedt E, Iwasaki A, Li H, Fu Y, Wang S, Xu H, Yamanouchi K. Rotational, vibrational, and electronic modulations in N_2^+ lasing at 391 nm: evidence of coherent $B^2\Sigma_u^+ - X^2\Sigma_g^+ - A^2\Pi_u$ coupling. *Phys Rev Lett.* 2019;123(20):203201.
9. Zhang X, Lu Q, Zhang Z, Fan Z, Zhou D, Liang Q, Yuan L, Zhuang S, Dorfman K, Liu Y. Coherent control of the multiple wavelength lasing of N_2^+ : coherence transfer and beyond. *Optica.* 2021;8:668.
10. Yao J, Wang L, Chen J, Wan Y, Zhang Z, Zhang F, Qiao L, Yu S, Fu B, Zhao Z, et al. Photon retention in coherently excited nitrogen ions. *Sci Bulletin.* 2021;66:1511.
11. Richter M, Lytova M, Morales F, Haessler S, Smirnova O, Spanner M, Ivanov M. Rotational quantum beat lasing without inversion. *Optica.* 2020;7:586.
12. Xu H, Lotstedt E, Iwasaki A, Yamanouchi K. Sub-10-fs population inversion in N_2^+ in air lasing through multiple state coupling. *Nat Commun.* 2015;6:8347.
13. Yao J, Jiang S, Chu W, Zeng B, Wu C, Lu R, Li Z, Xie H, Li G, Yu C, et al. Population redistribution among multiple electronic states of molecular nitrogen ions in strong laser fields. *Phys Rev Lett.* 2016;116(14):Article 143007.
14. Yao J, Zeng B, Xu H, Li G, Chu W, Ni J, Zhang H, Chin SL, Cheng Y, Xu Z. High-brightness switchable multiwavelength remote laser in air. *Phys Rev A.* 2011;84(5):051802.
15. Mysyrowicz A, Danylo R, Houard A, Tikhonchuk V, Zhang X, Fan Z, Liang Q, Zhuang S, Yuan L, Liu Y. Lasing without population inversion in N_2^+ . *APL Photonics.* 2019;4:110807.
16. Liu Y, Ding P, Lambert G, Houard A, Tikhonchuk V, Mysyrowicz A. Recollision-induced superradiance of ionized nitrogen molecules. *Phys Rev Lett.* 2015;115(13):Article 133203.
17. Lei H, Yao J, Zhao J, Xie H, Zhang F, Zhang H, Zhang N, Li G, Zhang Q, Wang X, et al. Ultraviolet supercontinuum generation driven by ionic coherence in a strong laser field. *Nat Commun.* 2022;13:4080.
18. Kleine C, Winghart M, Zhang Z, Richter M, Ekimova M, Eckert S, Vrakking M, Nibbering E, Rouzee A. Electronic state population dynamics upon ultrafast strong field ionization and fragmentation of molecular nitrogen. *Phys Rev Lett.* 2022;129:Article 123002.
19. Li G, Jing C, Zeng B, Xie H, Yao J, Chu W, Ni J, Zhang H, Xu H, Cheng Y, et al. Signature of superradiance from a nitrogen-gas plasma channel produced by strong-field ionization. *Phys Rev A.* 2014;89(3):Article 033833.
20. Miao Z, Zhong X, Zhang L, Zheng W, Gao Y, Jiang H, Gong Q, Wu C. Stimulated-Raman-scattering-assisted superfluorescence enhancement from ionized nitrogen molecules in 800-nm femtosecond laser fields. *Phys Rev A.* 2018;98(3):Article 033402.
21. Lewenstein M, Balcou P, Ivanov MY, L'Huillier A, Corkum PB. Theory of high-harmonic generation by low-frequency laser fields. *Phys Rev A.* 1994;49(3):2117.
22. Goulielmakis E, Loh ZH, Wirth A, Santra R, Rohringer N, Yakovlev VS, Zharebtsov S, Pfeifer T, Azzeer AM, Kling MF, et al. Real-time observation of valence electron motion. *Nature.* 2010;466(7307):739–743.
23. Zhang Y, Lötstedt E, Yamanouchi K. Population inversion in a strongly driven two-level system at far-off resonance. *J Phys B Atomic Mol Phys.* 2017;50(18):Article 185603.
24. Langhoff SR, Bauschlicher CW. Theoretical study of the first and second negative systems of N_2^+ . *J Chem Phys.* 1988;88(1):329–336.
25. Ott C, Kaldun A, Raith P, Meyer K, Laux M, Evers J, Keitel CH, Pfeifer T. Lorentz meets Fano in spectral line shapes: A universal phase and its laser control. *Science.* 2013;340(6133):716–720.
26. Limonov MF, Rybin MV, Poddubny AN, Kivshar YS. Fano resonances in photonics. *Nat Photon.* 2017;11(9):543–554.
27. Brewer RG, Shoemaker RL. Optical free induction decay. *Phys Rev A.* 1972;6(6):2001.
28. Chesnokov EN, Kubarev VV, Koshlyakov PV, Kulipanov GN. Direct observation of the terahertz optical free induction decay of molecular rotation absorption lines in the sub-nanosecond time scale. *Appl Phys Lett.* 2012;101(13):Article 131109.
29. Bengtsson S, Larsen EW, Kroon D, Camp S, Miranda M, Arnold CL, Huillier AL, Schafer KJ, Gaarde MB, Rippe L, et al. Space-time control of free induction decay in the extreme ultraviolet. *Nat Photon.* 2017;11(4):252–258.
30. Hahn EL. Nuclear induction due to free Larmor precession. *Phys Rev.* 1950;77(2):297.
31. Chu W, Zeng Z, Yao J, Xu H, Ni J, Li G, Zhang H, He F, Jing C, Cheng Y, et al. Multiwavelength amplified harmonic emissions from carbon dioxide pumped by mid-infrared femtosecond laser pulses. *Euro Phys Lett.* 2012;97(6):64004.

Multiple-Photon Resonance Enabled Quantum Interference in Emission Spectroscopy of N₂⁺

Xiang Zhang, Qi Lu, YaLei Zhu, Jing Zhao, Rostyslav Danylo, Liang Xu, Mingwei Lei, Hongbing Jiang, Chengyin Wu, Zhedong Zhang, Aurélien Houard, Vladimir Tikhonchuk, André Mysyrowicz, Qihuang Gong, Songlin Zhuang, Zengxiu Zhao, and Yi Liu

Citation: Zhang X, Lu Q, Zhu Y, Zhao J, Danylo R, Xu L, Lei M, Jiang H, Wu C, Zhang Z, et al. Multiple-Photon Resonance Enabled Quantum Interference in Emission Spectroscopy of N₂⁺. *Ultrafast Sci.* 2024;4:0051. DOI: 10.34133/ultrafastscience.0051

Quantum interference occurs frequently in the interaction of laser radiation with materials, leading to a series of fascinating effects such as lasing without inversion, electromagnetically induced transparency, Fano resonance, etc. Such quantum interference effects are mostly enabled by single-photon resonance with transitions in the matter, regardless of how many optical frequencies are involved. Here, we report on quantum interference driven by multiple photons in the emission spectroscopy of nitrogen ions that are resonantly pumped by ultrafast infrared laser pulses. In the spectral domain, Fano resonance is observed in the emission spectrum, where a laser-assisted dynamic Stark effect creates the continuum. In the time domain, the fast-evolving emission is measured, revealing the nature of free-induction decay arising from quantum radiation and molecular cooperativity. These findings clarify the mechanism of coherent emission of nitrogen ions pumped with mid-infrared pump laser and are found to be universal. The present work opens a route to explore the important role of quantum interference during the interaction of intense laser pulses with materials near multiple photon resonance.

Image

View the article online

<https://spj.science.org/doi/10.34133/ultrafastscience.0051>

Use of this article is subject to the [Terms of service](#)

Ultrafast Science (ISSN 2765-8791) is published by the American Association for the Advancement of Science, 1200 New York Avenue NW, Washington, DC 20005.

Copyright © 2024 Xiang Zhang et al.

Exclusive licensee Xi'an Institute of Optics and Precision Mechanics. No claim to original U.S. Government Works. Distributed under a [Creative Commons Attribution License 4.0 \(CC BY 4.0\)](#).